Pulmonary Hemodynamics Simulations Before Stage 2 Single Ventricle Surgery: Patient-Specific Parameter Identification and Clinical Data Assessment

Gregory Arbia,[1] Chiara Corsini,[2] Catriona Baker,[3] Giancarlo Pennati,[2] Tain-Yen Hsia,[3] and Irene E. Vignon-Clementel[1]

[1]INRIA Paris-Rocquencourt, Le Chesnay Cedex, France and UPMC Univ Paris 6, Laboratoire Jacques-Louis Lions, Paris, France; [2]Laboratory of Biological Structure Mechanics, Department of Chemistry, Materials and Chemical Engineering 'Giulio Natta', Politecnico di Milano, Milan, Italy; and [3]UCL Institute of Cardiovascular Science, and Great Ormond Street Hospital for Children, NHS Foundation Trust, London, UK

(Received 30 June 2014; accepted 10 January 2015; published online 22 January 2015)

INTRODUCTION

Single ventricle defects are a spectrum of congenital heart disorders resulting in only one functional ventricle. Several stages of palliative surgery are required to connect the systemic and pulmonary circulations to the single ventricular power source. Accurate modeling of patient-specific physiology for clinical decision-making requires the integration of the patient's clinical data into numerical simulations.[32] Computational fluid dynamics studies of single-ventricle (SV) conditions[7,31,33] have presented the crucial aspect of specifying the relevant boundary conditions. A common method to take into account the effect of the downstream domain is to couple 3D Navier–Stokes equations to electric-analog (also called zero-dimensional, lumped or reduced) models; or one-dimensional models of the peripheral

Address correspondence to Irene E. Vignon-Clementel, INRIA Paris-Rocquencourt, Le Chesnay Cedex, France and UPMC Univ Paris 6, Laboratoire Jacques-Louis Lions, Paris, France. Electronic mail: irene.vignon-clementel@inria.fr

For the Modeling of Congenital Hearts Alliance (MOCHA) Investigators.

circulation (e.g. for SV[8,20,31,32] and citing references). This allows one to obtain information about local fluid dynamics due to changes in anatomical features resulting from surgical operations.[9,13] Besides, when the 3D-0D model is closed loop, changes on and from the heart or other key systemic factors, can be evaluated from the known preoperative patient state and for these different virtual surgeries.[9,13] Nevertheless, such multiscale models need patient-specific parameters to be an effective tool for clinical support in surgical planning. The current work provides the parametrization of the 0D components that are in direct contact with the multibranched 3D model, where neither flow nor pressure are known.

In cases of pure zero-dimensional models, a number of methods for parameter identification were applied to minimal models of the adult systemic arterial circulation,[25,27] and submodeling or sensitivity analysis were suggested to reduce the identification complexity in closed-loop models of the whole cardiovascular system.[11,14,21,28] However, these methods cannot be applied easily to 3D-0D modeling because of very high computational costs. Considering multiscale models, a possible approach consists of manually tuning lumped parameters;[20] however, this simple method requires intuition regarding hemodynamics, and has been found to be infeasible if the 3D geometry has multiple branches. Automatic parameter estimation methods have thus been developed. In Ref. 26, six parameters of an aortic model were estimated with a quasi-Newton method to achieve some pressure and flow waveform features inside the 3D model. In Ref. 12, the Windkessel parameters of 3D bifurcating aneurysm were estimated with an adjoint-based method to match systolic, diastolic and average pressure differences. In Ref. 6, wall displacement values were used to estimate the stiffness of the 3D fluid-solid interaction idealized aneurysm model and its outlet proximal resistance, based on a sequential estimation approach. In Ref. 19, a dozen Windkessel parameters in a 3D coarctation model were estimated with a Kalman filter approach on a corresponding 0D surrogate model of the 3D-0D model, to match given flow and pressure waveforms inside the 3D domain.

These different methods, although effective, are demanding in terms of numerical implementation or numerical costs. They have the advantage, however, of matching time-varying measurements. Our first aim here, is to provide an automatic parameter estimation for multi-branched geometries, which complexity is coherent with the type of available data. As described in the next section, clinical measurements are limited in single ventricle patients (only a few months old) immediately prior to the second stage of surgery. Namely, classical identification of the outflow impedances (compliances and resistances) for each vascular branch cannot be achieved since complete arterial pressure and flow tracings are usually lacking, and sometimes only the average values are available.

An alternative approach was previously developed[4,29] consisting of two steps: (1) total downstream resistances are identified for each pulmonary outlet; (2) each resistance is properly split and compliances are derived using a morphometric approach, and according to literature scaling rules (e.g. relative role of arterial and venous vascular beds). In Ref. 29 a simple method was introduced to iteratively tune total resistances of the 3D model and match clinical inlet average pressure, inlet average flow and outlets' flow repartition. In contrast, within this work, we extend the method for more general pressure clinical data localization, as clinical data are rarely given at the specific 3D boundaries. This constitutes the first novelty of the current study.

Historically, very little CFD work has been performed in relation to stage 1 circulation in single ventricle physiology. In Ref. 15 authors investigated the effect of clinical parameters such as shunt, vasculature and heart rate on the Norwood procedure in a generic 0D model. More recently,[22] the authors presented computational hemodynamics simulations in the systemic circulation of one specific Norwood case with aortic arch repair and Damus–Kay–Stansel anastomosis. However, the distribution of flows among the outlets was not directly controlled since a zero pressure gradient method was applied at the end of very long extensions to recover a physiological pressure level. Ceballos *et al.* [8] and DeCampli *et al.* [10] focused on the systemic circulation of generic Hybrid Norwood configurations where the 3D boundary conditions came from a close-loop 0D model, to understand local hemodynamics and effects of aortic arch stenosis severity and a reverse Blalock–Taussig shunt on coronary and carotid perfusion. To the best of our knowledge, no computational study exists on patient-specific pulmonary hemodynamics in the presence of a systemic-to-pulmonary shunt and proper boundary conditions. The second aim of this study is hence to provide a first characterization of blood flow behavior in the distal anastomosis of the systemic-to-pulmonary shunt, and the connected pulmonary arteries over several bifurcations, in a number of different single ventricle patients scheduled for stage 2 surgery.

Finally, the third aim of this work is to provide some concrete examples of how patient-specific inte-gration of clinical data and computational modeling can provide interesting insights to clinicians.

The article continues with the Methods section to present the different steps of the algorithm, from clinical data to automatic parameter tuning. The

Results section demonstrates this framework for six pre-stage 2 single ventricle patients, reporting, in addition, their specific 3D hemodynamics. A discussion follows on methodological, biomechanical and clinical aspects.

METHODS

The Methods section presents the type of clinical data that define the patient-specific geometry and hemodynamics target values. The automatic tuning of reduced model parameters (i.e. total downstream resistances for each branch) to reach these target values is explained. In this work six patient-specific computational models were built to describe hemodynamics into the corresponding three-dimensional regions of interest, reflecting the patient state in coherence with the clinical measurements acquired before stage 2 surgery.

Clinical Cases

Patients A, B and C were recruited at the University of Michigan, Ann Arbor, MI, USA; patients D and E at Medical University of South Carolina, Charleston, SC, USA; and patient F recruited at Great Ormond Street Hospital, London, UK. The study was approved by the institutional review board at each institution and consent was obtained from the subject's legal guardian.

Patient A had a diagnosis of pulmonary atresia with intact ventricular septum. The stage 1 surgery comprised a central shunt, from the ascending aorta (AoA) to the main pulmonary artery (MPA). Patients B, C, D and F had hypoplastic left heart syndrome. Their stage 1 operations were all 3.5 mm right modified Blalock–Taussig shunts (rmBT). Patient E had tricuspid and pulmonary atresia, and underwent stage 1 surgery of a 4 mm rmBT, with additional left pulmonary artery augmentation to treat a left pulmonary artery stenosis. The patients' age and BSA are reported in Table 1.

Clinical Measurements

Pre-operative CMR and cardiac catheterization were performed prior to stage 2 surgery. Depending on institutional preference, CMR was either performed immediately prior to surgery under the same general anesthetic (GA); on the day of cardiac catheterization under the same GA with transfer between imaging suites; or in a hybrid CMR-catheterization imaging suite. For patients A, B and C, CMR was performed immediately prior to stage 2 surgery under the same GA, and cardiac catheterization was performed respectively 3 days, 1.5 months and 1 week prior to stage 2 surgery. CMR and cardiac catheterization were performed on the same day, 1.5 months prior to stage 2 surgery for patient D; and 1 month prior for patients E, and F.

CMR was performed on commercially available 1.5T scanners (Philips Intera Achieva, Best, Netherlands; Siemens Avanto, Siemens Medical Solutions, Erlangen, Germany) using a standardized protocol. CMR angiogram spatial resolution was 1.0 x 1.0 mm^2, with slice thickness 2.0mm (interpolated to 1.0mm). Contrast-enhanced CMR angiography was performed following injection of 0.2mmol/kg of intravenous gadoteridol (Prohance; Bracco Diagnostics, Princeton, NJ), using a routine clinical sequence to obtain 3D anatomical imaging. Free-breathing, electrocardiogram (ECG)-gated velocity-encoded phase contrast imaging sequences were used to acquire flow measurements, thus they give, in the best case scenario,

TABLE 1. Clinical measurements, numerical method and results.

Patient	A	B	C	D	E	F
Age (months)	6	4	5	5	3	4
BSA (m^2)	0.34	0.28	0.34	0.30	0.26	0.27
Inflow (cm^3/s)	7.5	12	20	9.7	12	16.6
Re_{max}	2,300	1,750	2,900	2,500	3,000	4,150
fs	0.64	0.46	0.55	0.46	0.67	0.52
PA pressure (mmHg)	12.8	12.7	13.5	12	17	11
$\Delta P_{L/R}$ (mmHg)	Negl.	Negl.	Negl.	Negl.	3	Negl.
Meas. location for tuning	Both	LPA	LPA	Both	RPA	Both
Control method	Average	Average	Average	Average	Min	Max
fs^{3D}	*0.64 (0.64)*	*0.46*	*0.55*	*0.46*	*0.66 (0.67)*	*0.52*
P_c^{3D} (mmHg)	*12.3 (12.4)*	*12.7*	*13.4*	*12.0*	*17.0 (17.0)*	*11.0*
$\Delta P_{L/R}^{3D}$ (mmHg)	*0.4 (0.4)*	*0.7*	*0.5*	*6.0*	*3.0 (3.0)*	*0.2*

For each patient, clinical data (age, BSA, average pulmonary inflow, deduced Reynolds number Re_{max}, flow split fs, target pulmonary artery pressure value, negligible or not left/right pulmonary pressure difference), tuning set-up (left or right pulmonary side, and control method to define P_c^{3D}), and numerical results are italicized (obtained flow split fs^{3D}, controlled pressure P_c^{3D} and pressure difference between left and right sides $\Delta P_{L/R}^{3D}$). Numbers are for the steady tuning and in parenthesis for the pulsatile tuning.

cycle-averaged time-varying information. For patients A and D, flows were measured in the branch pulmonary arteries; and for patients B, C, E and F, in the pulmonary veins, for which only time-averages are equal to the corresponding arterial flows. The total pulmonary flow (inflow) was obtained by adding the left and right sided pulmonary flows, and was imposed at the inlet surface (shunt). The mean values are reported in Table 1. All clinical data processing occurred at one core laboratory. Flow measurements were calculated using an in-house plug-in for OsiriX open-source software (OsiriX Foundation, Geneva, Switzerland).

Cardiac catheterization followed a routine clinical protocol and occurred under GA or sedation in a bi-plane fluoroscopy suite (Siemens Medical Solutions USA, Inc. Pennsylvania). A fluid-filled catheter system was used to acquire pressure in the common atrium and on the venous side, by a pulmonary venous wedge pressure as a surrogate of the pulmonary artery pressure (only cycle-averaged values can be used). Pressure differences between left and right sides ($\Delta P_{L/R}$) were measured and were considered negligible (0–1 mmHg) for patient A, B, D, F whereas for patient E it was 3mmHg. For patient C, the measurement was done on the left, and the pressure difference was assumed negligible (this case will be discussed later). These pulmonary artery pressures and left-right pressure differences are reported in Table 1.

Numerical Methods

The pre-operative anatomy of each patient was reconstructed from three-dimensional contrast enhanced CMR data using commercial software (Mimics, Mate-rialize, NV, Leuven, Belgium). The vascular region of interest (the distal shunt and the pulmonary arteries extending to their first branches) was selected to include enough branches to avoid numerical instabilities or to largely include the future virtual stage 2 operative anastomosis,[9,13] without going beyond the branches for which the image resolution would affect the simula-tion accuracy. A three-dimensional surface was thus obtained, following operations of segmentation and region-growing described in details in Refs. 3, 24. Figure 1 shows the reconstructed 3D geometries for the six patients. The inlet surface areas of patients A, B, C, D, E, and F are respectively 3.4×10^{-2}, 1.3×10^{-1}, 1.8×10^{-1}, 6.2×10^{-2}, 6.3×10^{-2} and $5.9 \times 10^{-2}\,\mathrm{cm}^2$.

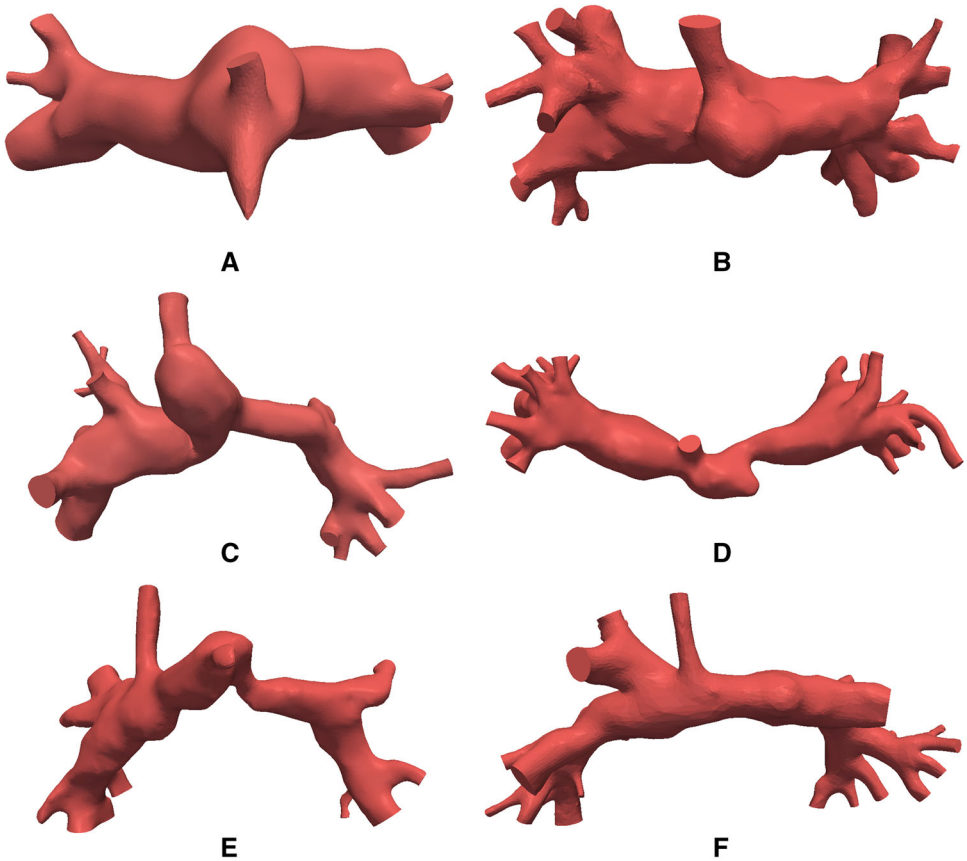

FIGURE 1. 3D geometrical model of patients A, B, C, D, E, F. The right (left) lung is on the left (right) for each patient.

For each of these 3D models, finite element meshes were generated with the commercial software MeshSim (Simmetrix Inc., Clifton Park, MY). Resulting meshes were anisotropically adapted to the flow in several steps.[17,23] The 3D meshes of patients A, B, C, D, E and F contain 715K, 970K, 1, 050K, 1, 500K, 710K and 1, 540K tetrahedra respectively.

In order to understand hemodynamics in these single ventricle geometries, and reflect the effect of the downstream vascular trees, rigid-wall Navier–Stokes equations were solved in three-dimensional models, coupled to zero-dimensional models (Fig. 2). This multi-domain approach and its monolithic numerical implementation are described in detail in Refs. 30, 31. All simulations were performed with the stabilized implicit finite element Navier–Stokes solver, SimVascular (http://simtk.org), assuming blood as an incompressible Newtonian fluid with a density of 1,060 kg m^{-3} and a dynamic viscosity of 0.004 Pa s.

Here, only simulations with total resistances (Ri) as outflow boundary conditions are presented, since reliable time-tracings to be applied at the inlet and in the atrium (Pat) are missing. The complete 5-parameter (RCRCR) impedance was used (data not reported) for virtual surgery of stage 2, in a closed-loop multiscale model, where proper boundary conditions for the whole pulmonary model were automatically provided by internal coupling.[4,13] A description of the simplified approach adopted to derive from the total downstream resistance the complete 5-parameter reduced model is described elsewhere.[1,4,29]

Tuning of Reduced Parameters

The main challenge of this study is to determine outflow boundary conditions for each patient-specific model that are consistent with the clinically measured data: (1) time-average flow distribution between left and right sides (flow split) denoted by fs and (2) time-average pulmonary arterial pressure denoted by P_t, which is the target pressure to match, and whose location and definition vary for each patient. The values defined as target pulmonary arterial pressures are reported in Table 1.

The automatic tuning of outflow boundary condition was introduced in Ref. 29 for patient-specific simulations of the stage 2 (bi-directional Glenn) procedure. It consisted of iteratively tuning a total resistance at each outlet by coupling 3D Navier–Stokes equations to a resistance with a fixed point method until recovering: (1) the measured transpulmonary gradient between the superior vena cava and the left atrium, and (2) the pulmonary flow split. Here, this method is extended in order to take into account the

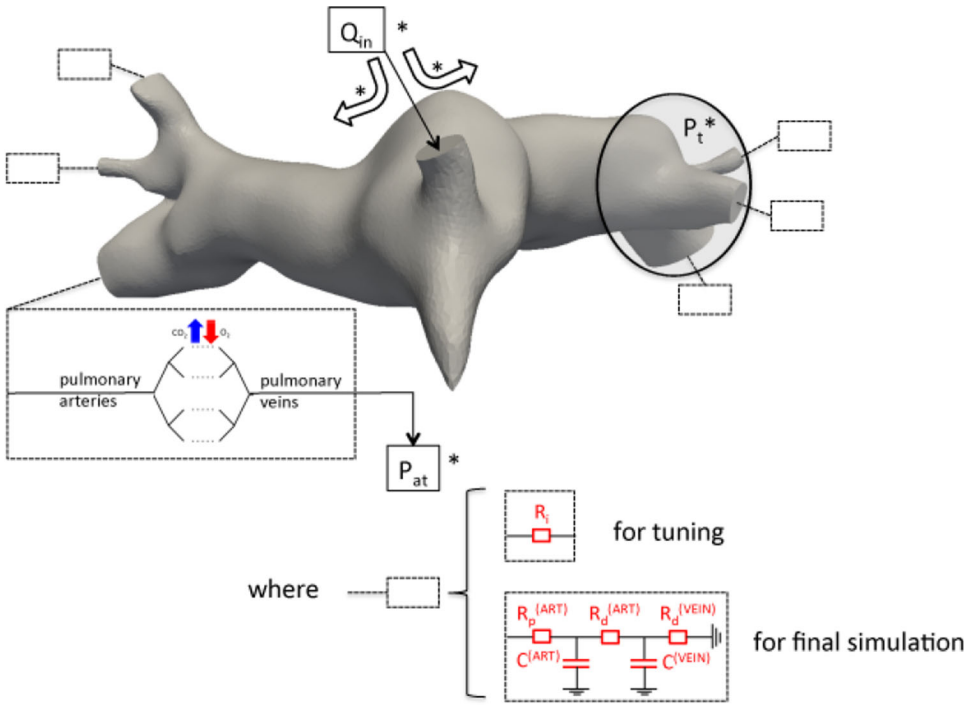

FIGURE 2. Multi-scale set-up, with the 3D domain, its inlet face on which the inflow Q_{in} is prescribed, and the distal pulmonary circulation for each outlet that all merge in the single atrium defined by its pressure P_{at}. Clinically measured quantities are marked with a star. At each outlet (dashed rectangle), the pulmonary arteries, capillaries and veins are represented either by a single total resistance for tuning, or by a more complete 5-parameter reduced model for virtual surgery.[1,4]

different locations of measured pulmonary arterial pressure: instead of only handling situations where the measured pressure coincides with the pressure at one boundary of the 3D domain (the inlet), the former can be more general, as will be explained below. This changes the way the outlet parameters are updated at each tuning iteration, and possibly the algorithm convergence.

The target flow split (fs) is computed from the time-average right pulmonary (Q_{R}) and left pulmonary (Q_{L}) CMR flows as follow:

$$\mathrm{fs} = \frac{Q_{\mathrm{R}}}{Q_{\mathrm{L}} + Q_{\mathrm{R}}} \tag{1}$$

The mean flow rate (Q_i), that is the target to reach through an outlet i, is assumed to be proportional to the surface area of this outlet (S_i):

$$Q_i \propto S_i \tag{2}$$

A power law could also be used if relevant.[29] A target average value for the flow rate at outlet i is thus a function of the inlet flow rate (Q_{in}) coming from clinical measurements:

$$Q_i = Q_{\mathrm{in}}\left(\delta_{i\mathrm{r}}\mathrm{fs} + (1-\delta_{i\mathrm{r}})(1-\mathrm{fs})\right)\frac{S_i}{\sum_j S_j\delta_{ij}} \tag{3}$$

where $\delta_{i\mathrm{r}}$ is the kronecker symbol equal to 1 if outlet i is on the right side and 0 if not, and δ_{ij} is the kronecker symbol equal to 1 if outlet j is on the same side as outlet i and 0 if not.

A first value of R_i at each outlet is estimated to initialize the algorithm. This serves as the boundary condition for a first 3D Navier–Stokes simulation that is run with sufficient time steps in order to reach stable state results: typically a few 100 time steps for steady simulations and four cardiac cycles for pulsatile simulations. Note here, that even in case of steady inlet flow (so called "steady simulations"), the resulting 3D flow is unsteady due to its complex interaction with the patient-specific geometry. Therefore, we use a transient formulation even for steady boundary conditions.

By post-processing the results over the last stable period, time-averaged (and mean in space) pressure ($P_i^{3\mathrm{D}}$) and flow rate ($Q_i^{3\mathrm{D}}$) are computed at each outlet. A flow split ($\mathrm{fs}^{3\mathrm{D}}$, based on the sum of the flows $Q_i^{3\mathrm{D}}$ on each side), and a controlled pressure ($P_c^{3\mathrm{D}}$) that varies according to the measurement location and clinician input, are then calculated. Note that the exact pressure measurement location was unknown, hence this controlled pressure could not be related to the output pressure at a specific location in the 3D domain. Rather, if catheterization was performed on the left pulmonary side, $P_c^{3\mathrm{D}}$ is the average pressure over all the outlets of the left side ($P_i^{3\mathrm{D}}$, $i \in [0, N]$ for N the number of left pulmonary outlets). Sometimes, there were several measurements done on one or both sides; $P_c^{3\mathrm{D}}$ is then defined with the clinical expert as being the maximum or the minimum value over all the corresponding branches of number N, e.g.

$$P_c^{3\mathrm{D}} = \min_i P_i^{3\mathrm{D}}, i \in [0, N] \tag{4}$$

These different options define *the measurement for tuning* and *control method* reported in Table 1. The results are then compared to the target pressure and flow values,

$$\begin{aligned} \varepsilon_P &= \frac{|P_t - P_c^{3\mathrm{D}}|}{P_t} \\ \varepsilon_Q &= \frac{1}{N}\sum_{i=1}^{N}\left(\frac{Q_i^{3\mathrm{D}} - Q_i}{Q_i} - \frac{1}{N}\sum_{i=1}^{N}\frac{Q_i^{3\mathrm{D}} - Q_i}{Q_i}\right)^2\Bigg)^{\frac{1}{2}} \end{aligned} \tag{5}$$

where N is the total number of outlets.

If convergence is not reached within a certain tolerance, the resistance at each outlet is updated as follows:

$$R_i = \frac{P_t - (P_c^{3\mathrm{D}} - P_i^{3\mathrm{D}})}{Q_i} \tag{6}$$

Another 3D simulation is run coupled to the new set of resistances R_i, where $i \in [0, N]$ for N outlets. This process is repeated until convergence.

In the case of a flow time-tracing being used as model inflow, pulsatile tuning simulations are performed, which better capture nonlinear effects across the 3D domain; total resistances (Ri) are also applied as boundary conditions, while pulsatile flow is imposed at the inlet. The controlled variables ($P_c^{3\mathrm{D}}$, $Q_i^{3\mathrm{D}}$) are then the time-averaged values over the last cardiac cycle. The framework presented above is the same for steady and pulsatile simulations. The steady tuning simulations were performed for all six patients, whereas the pulsatile ones only for patients A and E.

RESULTS

The Results section demonstrates this framework on six pre-stage 2 single ventricle patients, reporting how well the clinical data are matched, and presenting their local hemodynamics (3D pressure, flow and wall shear stress).

Parameter Tuning Results

Table 1 reports the tuning results. Steady tuning was run for every patient: the results ($\mathrm{fs}^{3\mathrm{D}}$ and $P_c^{3\mathrm{D}}$) are very close to the targeted clinical data. However, if we focus on the not targeted quantity ($\Delta P_{\mathrm{L/R}}$), the model

predictions are satisfactory only in five cases. Indeed, according to clinical observations, the pressure difference between right and left lungs was significant only for patient E, whereas the calculated $\Delta P^{3D}_{L/R}$ was significant for both patients E and D. This point will be considered in detail in the Discussion section. Figure 3 illustrates the convergence of the tuning algorithm for pressure and flow: both errors are under 2% for all patients, except for patient F where ϵ_Q is 5%. Pulsatile tuning was also performed for patients A and E and led to results (reported in parenthesis in Table 1) all very close to both steady tuning and targeted clinical values. As a consequence, the next paragraphs only report the 3D results of the steady tuning.

3D Hemodynamics

In Fig. 4 the pressure map for each patient is presented at the end of the tuning. We observe a high peak of pressure on the wall. The maximum pressure for patients A, B, C, D, E and F are respectively 52, 26, 25, 45, 62 and 74 mmHg. The patients A, B and F have homogeneous pressure in both pulmonary arteries respectively, approximately 12, 13 and 11 mmHg. Moreover, patients D and E have a left pulmonary artery (LPA) stenosis which involves a significant pressure loss of approximately 6 and 3 mmHg respectively, while homogeneous pressure is found in the right pulmonary artery (RPA). A last remark concerns patient C who has a kink in the RPA close to the shunt. The kink does not generate a significant pressure loss and pressure is homogeneous in both PAs, around 13.5 mmHg.

In Fig. 5 blood flow patterns for each patient are presented at the end of the tuning. A very complex flow can be observed in the 3D geometrical domain, especially close to the shunt where blood flow is the high-est. Highest velocity is obtained in the center of the shunt and is respectively equal to 470, 250, 265, 319, 377 and 570 cm/s. For patients A, B, and F the blood is swirling in the pulmonary arteries close to the shunt and goes towards the outlets smoothly with less complexity. This mixing flow behavior extends into the main pulmonary artery stump for patients B, C, and D where the stump from the ligated vessel is prominent. For patient E, swirling reflects the tortuous geometry on the left side, where there is a constriction anastomosis near the main pulmonary artery stump, followed by an LPA stenosis.

In Fig. 6 the wall shear stress surface maps are represented for each patient. For all patients the maximal wall shear stress is reached either in the shunt, or where there is a peak of pressure, respectively equal to 73.8, 55.3, 52.9, 66.3, 67.1, and 69.7 Pa. Moreover, for patients D and E, the stenosis involves a large wall shear stress respectively equal to 54.3 and 61.4 Pa. Regarding patient A, where the main pulmonary artery was ligated the mean wall shear stress is 57.8 Pa, which is high compared to the rest of the domain. In contrast, in the corresponding location of patient E, the mean wall shear stress is close to 0. Comparing patients B and C, which have a similar shape, the obtained mean wall shear stress is respectively equal to 17 and 40 Pa.

DISCUSSION

Methodology Discussion

This proposed methodology to tune reduced model parameters, adopted as outlet boundary conditions of patient-specific 3D pulmonary arterial models, accurately replicates clinical measurements (Table 1), within acceptable clinical measurement tolerance lim-its. As the pressure difference between the left and right side was not used for parameter tuning, the fact that this measurement is well-matched by the simulations constitutes a preliminary validation of the results.

At the 3D outlets, it would not be relevant to apply pressure boundary conditions for the following reasons: (1) the measured flow distribution between the two different lungs cannot be easily matched, and (2) the pressure measurements were not performed at these locations in the pulmonary arteries. Sometimes,

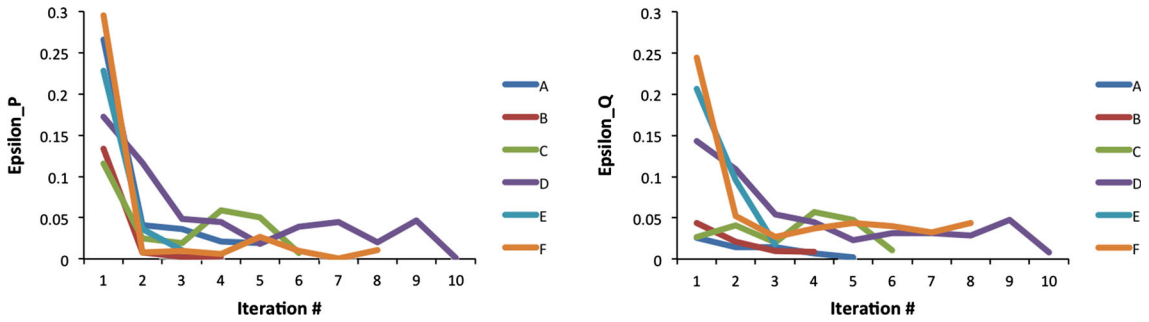

FIGURE 3. Convergence of the tuning algorithm shown for pressure (ϵ_P) and flow (ϵ_Q) for patients A–F.

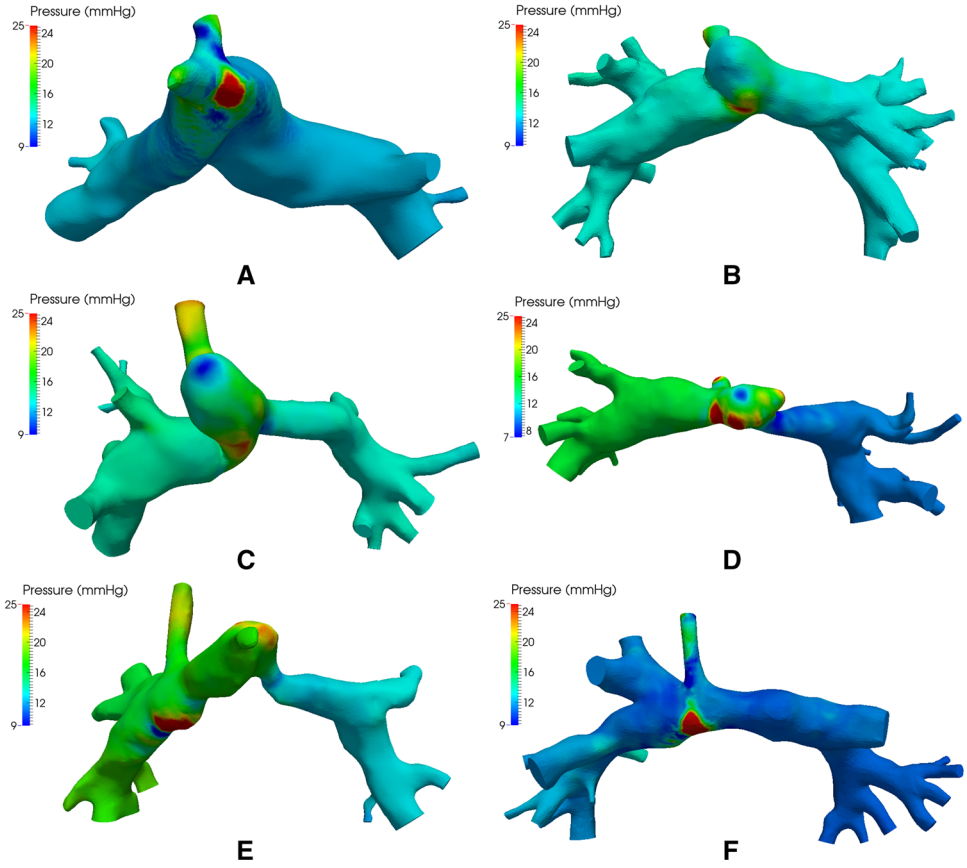

FIGURE 4. Pressure maps for patients A–F. Maximum pressure is equal to 25 mmHg on the color scale, even if the real maximal pressure is larger. 1 mmHg = 133.3 Pa.

applying the same pressure at all outlets can even lead to unphysiological reverse average flow in some of the branches. Applying time-varying flow boundary conditions would also be difficult because the flow distribution between the different outlets is not necessarily constant, and would not guarantee coherence with the pressure measurements. Moreover, prescribing pressure or flow reduces the predictive potential such as in virtual surgery planning.[32] This is why we coupled 3D Navier–Stokes equations to reduced models.

The tuning methodology introduced in this work consists of coupling Navier–Stokes equations to reduced models (here resistances) at the outlets and running steady or pulsatile simulations. The *a priori* interest in running a pulsatile simulation is the integration of all non linearities due to the 3D geometrical model, and to obtain a more accurate set of reduced model parameters. However, to achieve periodic stability, pulsatile simulations need to be run over 4 cardiac cycles (around 2,000 time steps) and the iterative process converges within 5 iterations, thus around 10,000 time steps. In comparison, 100 time steps for a steady stimulation were enough and the iterative process converges in 5 iterations (tolerance of 0.05), thus around 500 time steps were necessary in total. Furthermore, pulsatile tuning for patients A and E was performed, and both matched targeted clinical values were very close to the steady tuning results. Moreover, the reduced model parameters were very close to those obtained by steady tuning. Indeed, for patients A and E the difference between steady and pulsatile tuning are respectively 6.37 and 7.82% in resistances, computed by the formula (5).

The first source of uncertainty comes from the geometrical reconstruction for these young babies. The typical pixel size from 3D CMR angiography is $1 * 1\ mm^2$. In addition 3D CMR angiography may suffer from signal loss in areas of turbulent or complex flow. Thus, including or excluding a pixel in a small area region, such as a shunt stenosis, may lead to errors in the 3D geometry. This kind of uncertainty should be addressed in future work. Where available, 2D CMR black blood imaging sequences were used to check diameters at specific locations since spatial res-olution is higher in this sequence. As a final check for each patient, a comparison was made between the 3D reconstruction and the 2D bi-planar fluoroscopy images acquired in the cardiac catheter laboratory.

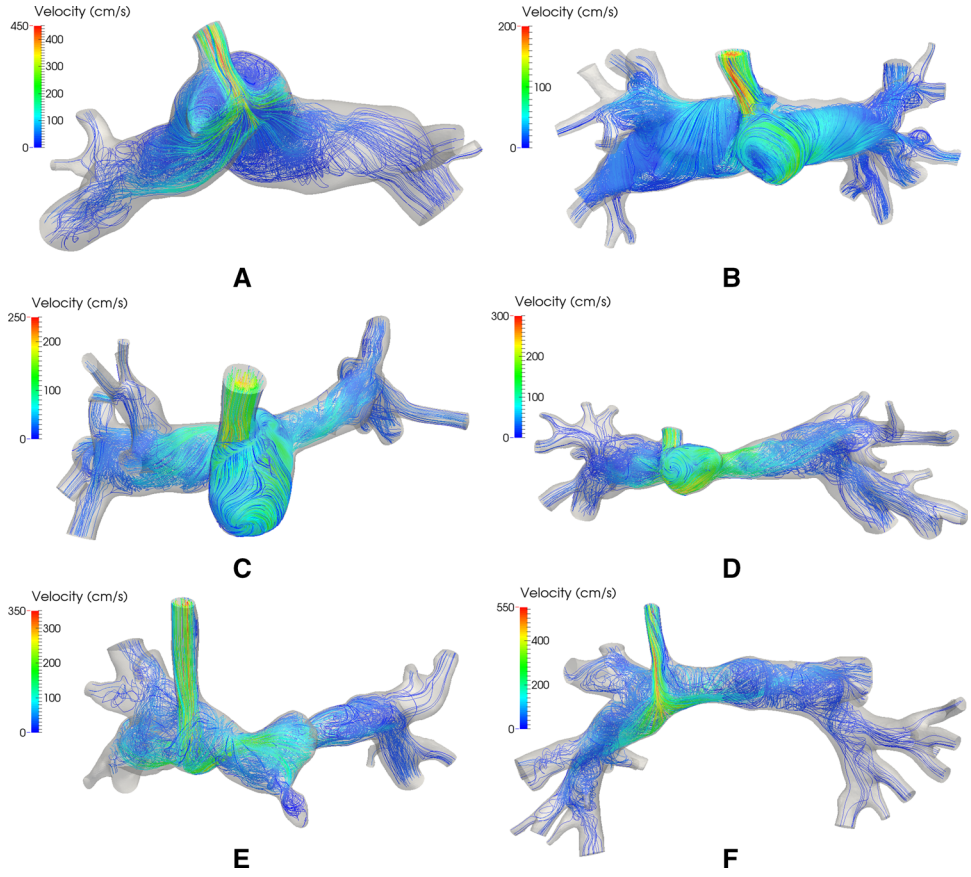

FIGURE 5. Streamlines of patients A–F colored by velocity magnitude.

Patient D had the appearance of luminal narrowing with an obvious distal stenosis on catheter angiographic sequences. The 2D measurements were used to adjust the 3D reconstruction to give an accurate representation of the geometry in this region.

Branching bifurcations were included evenly on both sides, and at a branch level coherent with image resolution. Although a large number of branches increases computational time, cutting the branches before the first bifurcations on each side often leads to numerical instabilities, as was tested for patient A. Stabilizing the numerical scheme is then warranted.[2,16] Note that sometimes, as was the case for patient F, the robust convective stabilization was not enough to avoid numerical divergence in the short model. Besides, as cutting branches or stabilization can change flow features close to the boundary, it is necessary to include enough branches to not affect the flow close to the current anastomosis or the one of the next stage virtual surgery.

Furthermore, in this work walls of the 3D geometrical models were assumed to be rigid because data for the heterogeneous assessment of the wall parameters were not known. Moreover, the shunt is a rigid graft and the anastomosis is also quite rigid because of sutures. If time-varying geometry data were available, the elasticity parameters could also be inferred.[6] However, it has been shown that FSI has little effect at rest at least at later stage of the palliation.[5]

Regarding the inlet boundary condition, since the velocity profile was not available, a parabolic profile was imposed at the inlet, which is commonly used for blood flow in arteries. We verified in one case that changing the profile to a flat velocity profile did not significantly change the pressure or the velocity fields.

Biomedical Significance of the Results

The results of this study highlight the high complexity of the blood flow patterns in pulmonary arteries in single ventricle patients approaching stage 2 surgery with a systemic-to-pulmonary artery shunt in situ. The variability of the pulmonary flow rate—between 7.5 and 20 cm^3/s—leads to very high Reynolds numbers, between 1, 750 and 4, 150 when computed at the shunt inlet with the maximum velocity.

This leads to values of wall shear stress that are very high. They are in the same order of magnitude as in the aorta of a typical Norwood patient[22] (keeping in mind

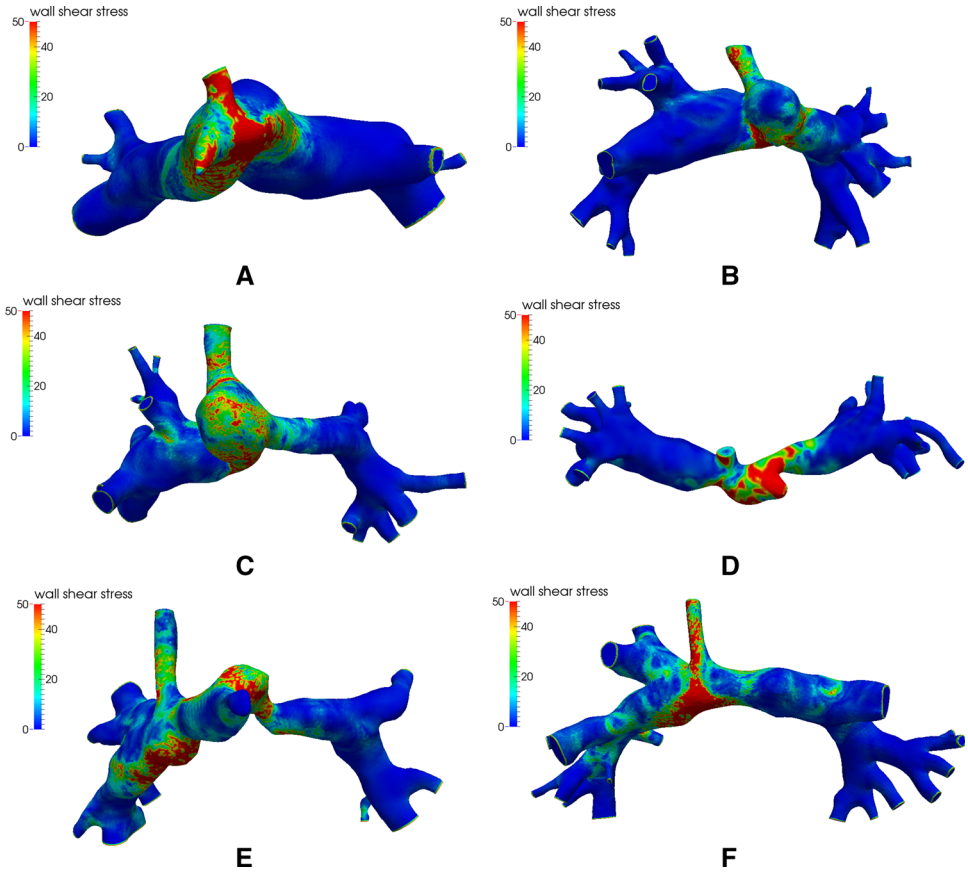

FIGURE 6. Wall shear stress map of patients A–F in Pa. Maximum color scale is fixed at 50 Pa but the real maximum value is larger.

that the shunt is a direct connection from the aorta or brachial artery). In the Glenn circulation,[29] a typical wall shear stress is more than 10 times lower. For patients B and C, the main pulmonary artery was ligated, forming a sphere bulging out of the ligation site, which might foster recirculation, and thus lower wall shear stress. Yet, the computed wall shear stresses were quite different. The relative differences in wall shear stress between patients may have some bearing on the development of the PAs; however, the stage 1 circulation is only present for a few months before second stage palliative surgery is required. Therefore, these effects will be of a fairly short duration.

The importance of the severe PA stenosis causing a pressure drop, and the swirling behavior of the blood flow was also shown. This complexity is induced by the high Reynolds number in the shunt. For these stenosis cases and patient C with its PA kinks, computational fluid dynamics complements information from clinical measurements. One potential clinical application for this technique is to aid clinicians' understanding of the significance of anatomical abnormalities in these complex patients.

For example, patient C appears to have a significant geometric 'kink' or restriction in their RPA, just distal to the shunt. Only a distal LPA pressure measurement was obtained clinically, so the hemodynamic effect of this lesion was unknown. However, simulation results clearly indicate that the pressure difference between the shunt anastomosis and the PAs are equal on the left and right sides. This was of interest to the clinicians, as the consensus was that judging by the anatomy alone, they would expect a pressure loss across the RPA. Indeed, at stage 2 surgery, patients A, C, D, and E all underwent patch augmentation of their central PAs or proximal LPAs judged on the appearance of the geometry alone. This work suggests that in some cases the clinician's perception of what constitutes a geometric abnormality may actually not result in a hemodynamically significant pressure difference, as in case C. Although, the tortuous course of the PA appears to constitute a stenosis, it is partly an illusion due to the distal PA having a relatively large cross-sectional area.

For patient D, the first attempt was to match the measured flow split of 0.46 and a pressure on both

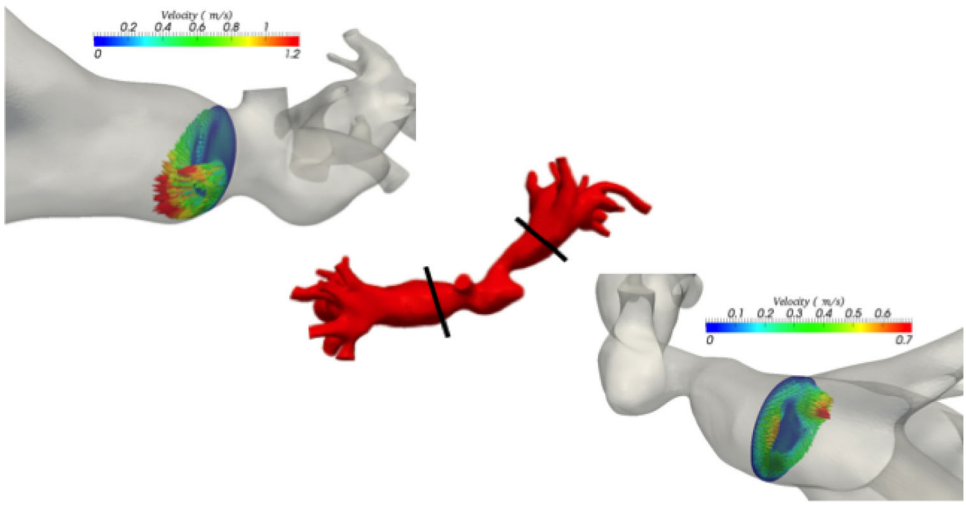

FIGURE 7. Velocity vectors (colured by their magnitudes) from the 3D simulation shown at the locations where the CMR flow measurements were performed.

LPA and RPA sides equal to 12 mmHg. Unfortunately, setting target flow split as 0.46 induced a pressure difference between the left and right sides of approximately 6 mmHg, which was not acceptable from a clinical point of view. Discussions with clini-cians led us to disregard the clinically measured flow split. By imposing the same average pressure on both sides, a flow split of 0.54 (more flow to the right side) was then found, which was clinically acceptable. The differences in flow split would correspond to an error of 0.78 ml/s (i.e. 8%) in estimating flow with CMR. This example highlights the impact of uncertainty of measurements on the numerical simulations. It could be interesting to investigate more precisely the effect of uncertainties of pressure and flow split measurements on the pressure loss through the stenosis. This patient-specific example was thus challenging and required a close collaboration with clinicians. On the other hand, performing simulations underlined the potential for incoherence of the original clinical measurements ; and joint assessment with clinical experts elucidated which data was more reliable to utilise.

The clinical hemodynamics measurements have uncertainties and it would be interesting to take this into account in future work.[29] Indeed, it would be useful to investigate their effect on the pressure loss through stenoses, and on the set of reduced model parameters.

A last comment regarding uncertainties of clinical measurements: in Fig. 7 simulated velocity vectors for patient D are shown at the same locations as flow measurements were performed in CMR. We highlight the complexity of the blood flow patterns at these locations, which might explain the difficulty obtaining accurate clinical time-varying velocity measurements by CMR at these locations. The PAs are relatively small, and are receiving flow from the aorta, or one of its branches, at high pressure. CMR flow measurements are typically less reliable in areas of complex flow because unpredictable phase shifts occur. This often leads to signal loss (voiding) and inaccurate flow measurements.[18] Typically, the PA flow measurements in this location would be underestimated in pre-stage 2 patients. The pulmonary veins may represent a more stable location to measure the pulmonary flow split, however, the physiology of these patients sometimes leads to the pulmonary veins receiving additional blood flow external to the pulmonary arteries. It is only through the iterative process of comparing simulation results to clinical measurements that suitable strategies for managing measurement uncertainty are reached.

CONCLUSION

In this work we develop a method to iteratively tune parameters of reduced models of 3D blood flow simulations in order to reflect the effect of the downstream vasculature, taking into account clinical measurements of pre-stage 2 single ventricle patients before undergoing the next palliative operation. This method was effectively demonstrated on six patients. It can be useful in other multi-branched blood flow simulations for which pressure or flow measurements are taken at various locations, and chosen to be matched as a minimum, maximum, average or other combinations of values in a given region.

Simulations in these pre-stage 2 cases highlighted the complexity of the blood flow patterns into the shunt anastomosis and the pulmonary arteries, as well as the very specific pressure map. The wall shear stress was found to be very high in magnitude, but varying in space differently according to the patients anatomy,

not necessarily leading to a low value in the ligated main pulmonary stump.

Simulations also assessed the effects of anatomical kinks or stenoses, demonstrating the potential use of the technique: clinicians do not always know whether a lesion is hemodynamically significant. These types of simulations could be helpful when planning whether to intervene on a PA anatomical problem. It involves more extensive surgery to intervene on a PA stenosis, so if clinicians better understood the difference between a significant stenosis and an anatomical anomaly that does not have an effect, it would save time and risk intervening when it was not necessary.

This methodology is, moreover, integrated into closed-loop multi-scale models for virtual surgical planning testing different surgical approaches.[4,9,13] It is also shown to be a tool for clinicians to assess coherence of clinical measurements: the iterative approach comparing clinical data to simulation results emerged as an effective strategy to understand clinical measurement limitations, and decide upon a strategy to replicate the clinical case such that it is compatible with clinicians' experience and expectations. This process highlights the impact of uncertainty quantification of the clinical measurements.

Finally, this first work on single ventricle shunt anastomoses at pre-stage 2 could be used to compare hemodynamics of different stages of the Fontan palliation.

ACKNOWLEDGMENTS

This work was supported by the Leducq Foundation as part of the Transatlantic Network of Excellence for Cardiovascular Research "Multi-scale modeling of single ventricle hearts for clinical decision support", and by the Associated team Cardio INRIA grant.

CONFLICT OF INTEREST

There is no conflict of interest for this work.

STATEMENT OF HUMAN STUDIES

Regarding human studies, the study was approved by the institutional review board at each institution (see "Methods" section) and consent was obtained from the subject's legal guardian.

STATEMENT OF ANIMAL STUDIES

No animal studies were performed.

REFERENCES

[1]Arbia, G. Multiscale modeling of blood flow in the context of congenital heart disease. Ph.D. thesis, UPMC Université Paris 6, Ecole doctorale de mathématiques de Paris Centre, 2014.

[2]Arbia, G., I. E. Vignon-Clementel, T. Y. Hsia, J. F. Gerbeau. Modified Navier-Stokes equations for the outflow boundary conditions in hemodynamics (submitted).

[3]Armillotta, A., P. Bonhoeffer, G. Dubini, S. Ferragina, F. Migliavacca, G. Sala, S. Schievano. Use of rapid prototyping models in the planning of percutaneous pulmonary valved stent implantation. *Proc. Inst. Mech. Eng. Part H J. Eng. Med.* 221(4), 407–416, 2007. doi:10.1243/09544119JEIM83.

[4]Baretta, A. Patient-specific modeling of the cardiovascular system for surgical planning of single-ventricle defects. Ph.D. thesis, Politecnico di Milano, Milan, Italy, 2014.

[5]Bazilevs, Y., M. C. Hsu, D. J. Benson, S. Sankaran, A. L. Marsden. Computational fluid-structure interaction: methods and application to a total cavopulmonary connection. *Comput. Mech.* 45(1), 77–89, 2009. doi:10.1007/s00466-009-0419-y.

[6]Bertoglio, C., P. Moireau, J. F. Gerbeau. Sequential parameter estimation for fluid–structure problems: Application to hemodynamics. *Int. J. Numer. Method. Biomed. Eng.* 28(4), 434–455, 2012.

[7]Bove, E.L., M. R. de Leval, F. Migliavacca, G. Guadagni, G. Dubini. Computational fluid dynamics in the evaluation of hemodynamic performance of cavopulmonary connections after the Norwood procedure for hypoplastic left heart syndrome. *J. Thorac. Cardiovasc. Surg.* 126(4), 1040–1047, 2003.

[8]Ceballos, A., I. R. Argueta-Morales, E. Divo, R. Osorio, C. A. Caldarone, A. J. Kassab, W. M. Decampli. Computational analysis of hybrid norwood circulation with distal aortic arch obstruction and reverse blalock-taussig shunt. *Ann. Thorac. Surg.* 94(5), 1540–50, 2012. doi:10.1016/j.athoracsur.2012.06.043.

[9]Corsini, C., C. Baker, E. Kung, S. Schievano, G. Arbia, A. Baretta, G. Biglino, F. Migliavacca, G. Dubini, G. Pennati, A. L. Marsden, I. Vignon-Clementel, A. M. Taylor, T. Y. Hsia, A. Dorfman. An integrated approach to patient-specific predictive modeling for single ventricle heart palliation. *Comput. Methods Biomech. Biomed. Engin. (June)*. 37–41, 2013. doi:10.1080/10255842.2012.758254.

[10]DeCampli, W.M., I. R. Argueta-Morales, E. Divo, A. J. Kassab. Computational fluid dynamics in congenital heart disease. *Cardiol Young* 22(6), 800–808, 2012. doi:10.1017/S1047951112002028.

[11]Hann, C.E., J. G. Chase, T. Desaive, C. B. Froissart, J. Revie, D. Stevenson, B. Lambermont, A. Ghuysen, P. Kolh, G. M. Shaw. Unique parameter identification for cardiac diagnosis in critical care using minimal data sets. *Comput. Methods Progr. Biomed.* 99(1), 75–87, 2010. doi:10.1016/j.cmpb.2010.01.002.

[12]Ismail, M., W. A. Wall, M. W. Gee. Adjoint-based inverse analysis of windkessel parameters for patient-specific vascular models. *J. Comput. Phys.* 244(0), 113–130, 2013. doi:10.1016/j.jcp.2012.10.028.

[13]Kung, E., A. Baretta, C. Baker, G. Arbia, G. Biglino, C. Corsini, S. Schievano, I. E. Vignon-Clementel, G. Dubini, G. Pennati, *et al.* Predictive modeling of the virtual Hemi-Fontan operation for second stage single ventricle palliation: two patient-specific cases. *J. Biomech.* 46(2), 423–429, 2013.

[14]Liang, F., K. Sughimoto, K. Matsuo, H. Liu, S. Takagi. Patient-specific assessment of cardiovascular function by

combination of clinical data and computational model with applications to patients undergoing fontan operation. *Int. J. Numer. Method Biomed. Eng.* 30(10), 1000–1018, 2014. doi:10.1002/cnm.2641.

[15]Migliavacca, F., G. Pennati, G. Dubini, R. Fumero, R. Pietrabissa, G. Urcelay, E. L. Bove, T. Y. Hsia, M. R. de Leval. Modeling of the Norwood circulation: effects of shunt size, vascular resistances, and heart rate. *Am. J. Physiol.—Hear. Circ. Physiol.* 280(5), H2076–H2086, 2001.

[16]Moghadam, M. E., Y. Bazilevs, T. Y. Hsia, I. E. Vignon-Clementel, A. L. Marsden. A comparison of outlet boundary treatments for prevention of backflow divergence with relevance to blood flow simulations. *Comput. Mech.* 48(3), 277–291, 2011.

[17]Muller, J., O. Sahni, X. Li, K. E. Jansen, M. S. Shephard, C. A. Taylor. Anisotropic adaptive finite element method for modelling blood flow. *Comput. Methods Biomech. Biomed. Eng.* 8(5), 295–305, 2005. doi:10.1080/10255840500264742.

[18]Oshinski, J.N., D. N. Ku, R. I. Pettigrew. Turbulent fluctuation velocity: the most significant determinant of signal loss in stenotic vessels. *Magn. Reson. Med.* 33(2), 193–199, 1995. doi:10.1002/mrm.1910330208.

[19]Pant, S., B. Fabreges, J. F. Gerbeau, I. E. Vignon-Clementel. A methodological paradigm for patient-specific multiscale CFD simulations: from clinical measurements to individual predictions. *Int. J. Numer. Method Biomed. Eng.* 30(11), 1614–1648, 2014.

[20]Pennati, G., C. Corsini, D. Cosentino, T. Y. Hsia, V. S. Luisi, G. Dubini, F. Migliavacca. Boundary conditions of patient-specific fluid dynamics modelling of cavopulmonary connections: possible adaptation of pulmonary resistances results in a critical issue for a virtual surgical planning. *Interface Focus* 1(3), 297–307, 2011. doi:10.1098/rsfs.2010.0021.

[21]Pope, S. R., L. M. Ellwein, C. L. Zapata, V. Novak, C. T. Kelley, M. S. Olufsen. Estimation and identification of parameters in a lumped cerebrovascular model. *Math. Biosci. Eng.* 6(1), 93–115, 2009.

[22]Qian, Y., J. L. Liu, K. Itatani, K. Miyaji, M. Umezu. Computational hemodynamic analysis in congenital heart disease: simulation of the norwood procedure. *Ann. Biomed. Eng.* 38(7), 2302–2313, 2010. doi:10.1007/s10439-010-9978-5.

[23]Sahni, O., J. Muller, K. Jansen, M. Shephard, C. Taylor. Efficient anisotropic adaptive discretization of the cardiovascular system. *Comput. Methods Appl. Mech. Eng.* 195, 5634–5655, 2006. doi:10.1016/j.cma.2005.10.018.

[24]Schievano, S., F. Migliavacca, L. Coats, S. Khambadkone, M. Carminati, N. Wilson, J. E. Deanfield, P. Bonhoeffer, A. M. Taylor. Percutaneous pulmonary valve implantation based on rapid prototyping of right ventricular outflow tract and pulmonary trunk from MR data. *Radiology* 242(2), 490–497, 2007. doi:10.1148/radiol.2422051994.

[25]Segers, P., E. R. Rietzschel, M. L. De Buyzere, N. Stergiopulos, N. Westerhof, L. M. Van Bortel, T. Gillebert, P. R. Verdonck. Three- and four-element windkessel models: assessment of their fitting performance in a large cohort of healthy middle-aged individuals. *Proc. Inst. Mech. Eng. H* 222(4), 417–428, 2008.

[26]Spilker, R. L., C. A. Taylor. Tuning multidomain hemodynamic simulations to match physiological measurements. *Ann. Biomed. Eng.* 38(8), 2635–2648, 2010. doi:10.1007/s10439-010-0011-9.

[27]Stergiopulos, N., B. E. Westerhof, N. Westerhof. Total arterial inertance as the fourth element of the windkessel model. *Am. J. Physiol.* 276(1 Pt 2), H81–H88, 1999.

[28]Sughimoto, K., F. Liang, Y. Takahara, K. Mogi, K. Yamazaki, S. Takagi, H. Liu. Assessment of cardiovascular function by combining clinical data with a computational model of the cardiovascular system. *J. Thorac. Cardiovasc. Surg.* 145(5), 1367–72, 2013. doi:10.1016/j.jtcvs.2012.07.029.

[29]Troianowski, G., C. A. Taylor, J. A. Feinstein, I. E. Vignon-Clementel, *et al.* Three-dimensional simulations in Glenn patients: clinically based boundary conditions, hemodynamic results and sensitivity to input data. *Trans. ASME-K-J. Biomech. Eng.* 133(11), 111,006, 2011.

[30]Vignon-Clementel, I. E., C. Alberto Figueroa, K. E. Jansen, C.A. Taylor. Outflow boundary conditions for three-dimensional finite element modeling of blood flow and pressure in arteries. *Comput. Methods Appl. Mech. Eng.* 195(29–32), 3776–3796, 2006. doi:10.1016/j.cma.2005.04.014.

[31]Vignon-Clementel, I. E., C.A. Figueroa, K. E. Jansen, C. A. Taylor. Outflow boundary conditions for 3D simulations of non-periodic blood flow and pressure fields in deformable arteries. *Comput. Methods Biomech. Biomed. Eng.* 13(5), 625–640, 2010. doi:10.1080/10255840903413565.

[32]Vignon-Clementel, I. E., A. L. Marsden, J. A. Feinstein. A primer on computational simulation in congenital heart disease for the clinician. *Prog. Pediatr. Cardiol.* 30(1), 3–13, 2010.

[33]de Zélicourt, D. A., A. Marsden, M. A. Fogel, A. P. Yoganathan. Imaging and patient-specific simulations for the Fontan surgery: current methodologies and clinical applications. *Prog. Pediatr. Cardiol.* 30(1), 31–44, 2010.